Left-handed metamaterials: The fishnet structure and its variations

M. Kafesaki,[1,2] I. Tsiapa,[1] N. Katsarakis,[1,3] Th. Koschny,[1,4] C. M. Soukoulis,[1,2,4] and E. N. Economou[1,5]
[1]*Institute of Electronic Structure and Laser (IESL), Foundation for Research and Technology Hellas (FORTH), P.O. Box 1527, 71110 Heraklion, Crete, Greece*
[2]*Department of Materials Science and Technology, University of Crete, 71003 Heraklion, Crete, Greece*
[3]*Science Department, Technological Educational Institute of Crete, 71004 Heraklion, Crete, Greece*
[4]*Ames Laboratory and Department Physics and Astronomy, Iowa State University, Ames, Iowa 50011, USA*
[5]*Department of Physics, University of Crete, 71003 Heraklion, Crete, Greece*
(Received 24 January 2007; published 19 June 2007)

We investigate, both theoretically and experimentally, a left-handed metamaterial design composed of pairs of short slabs connected with continuous wires, operating in microwave frequency regime. The design was found to give left-handed behavior for a wide range of structure parameters, maintaining high impedance match with free space. We introduce a capacitor-inductor circuit description of the design and we show that this description can account for all the characteristics of its electromagnetic behavior, explaining also its superior performance.

DOI: 10.1103/PhysRevB.75.235114 PACS number(s): 41.20.Jb

I. INTRODUCTION

Left-handed metamaterials are artificial composite structures that exhibit a homogeneous effective permittivity ϵ and permeability μ, which become negative over a common frequency range.[1,2] Such metamaterials can be constructed from nonmagnetic but conductive metals and dielectrics.

Since the experimental demonstration of the first left-handed metamaterial,[3] which was a combination of split-ring resonators[4] (SRRs) and continuous wires and was designed following ideas by Pendry *et al.*,[4,5] the operation frequency range of left-handed materials has been pushed upward from the initial lower gigahertz range,[3,6,7] to almost optical frequencies (see, e.g., Refs. 8–10), although in the latter the losses are considerable and the freedom to manipulate the desired features is very limited.

In Fig. 1, we show some of the basic structures being designed, simulated, fabricated, and tested for left-handed (LH) behavior. The basic idea to obtain negative permeability in all these structures is to create a hopefully strong magnetic resonance at a frequency $\omega=\omega_m$ by exciting resonant circular currents; this basic process can be simulated by an effective *LC* circuit exhibiting a resonance at $\omega_m=1/\sqrt{LC}$. If the resonance is strong enough and weakly damped, there would be a frequency range $\omega_1 \leqslant \omega \leqslant \omega_2$ $(\omega_m < \omega_1)$ where the real part of the permeability, $\mu_1(\omega)$, should be negative and the imaginary part, $\mu_2(\omega)$, should be very small, $\mu_2(\omega)/\mu_1(\omega) \ll 1$. The continuous wire appearing in all the structures of Fig. 1 is used to provide the negative ϵ response.[5] A system of such parallel wires exhibits a Drude-like plasmonic behavior for the permittivity, of the form $\epsilon(\omega)=1-\omega_p^2/\omega^2$, where the plasma frequency ω_p can be tailored by choosing the distance between the wires and the size of their cross section;[5] actually, the simple Drude-like behavior is modified because the elements providing the magnetic response behave electrically as short wires in the electric-field directions. The main effect of this modification in the lower-frequency part of the spectrum[11] is to lower the plasma frequency from ω_p to ω_p', such that $\epsilon(\omega_p')=0$ and $\epsilon(\omega)<0$ for $\omega<\omega_p'$.

From the structures shown in Fig. 1, the one of panel (a) is the original SRR&wire design proposed by Pendry *et al.* and implemented by Smith *et al.*,[3] which shows LH behavior for incident plane waves with electric field polarized parallel to the continuous wire and magnetic field perpendicular to the SRR; various modifications of that design were proposed in the literature, aiming mainly to make the structure simpler or more isotropic and appropriate for two-dimensional and three-dimensional LH materials. One of those modifications is shown in panel (b).

The structures of panels (c)–(f) can be considered as combinations of pairs of short slabs with continuous wires. As has been shown in earlier works,[8] the pair of short slabs provides a resonant magnetic response analogous to that of the SRR, associated with strong antiparallel currents in the two slabs of the pair. The main advantages of the slab-pair design compared to the SRR are its simplicity and its ability to produce LH behavior for incidence normal to the plane where such slabs are printed and/or deposited, enabling thus strong LH response with only one slab layer; this last feature can be exploited in the design and demonstration of high-frequency LH materials. Combining the pairs of slabs with continuous wires, one can obtain LH behavior, as is shown in Refs. 12 and 13 for the structure of Fig. 1(c).

The same concept of slabs and continuous wires is behind the structure of Fig. 1(d), known as the fishnet design,[10,14] which is the subject of the present paper. In the fishnet design, the slabs are as wide as the unit cell (along the *x* direction in Fig. 1, hence contiguous in the *x* direction due to the periodic repetition of the unit cell), something that does not significantly affect the frequency of their magnetic response, as is shown in Ref. 15; the slabs are physically connected with the continuous wires that provide the plasmonic electric response. This connection, as we will show in the present paper, leads to a superior performance of the fishnet design compared to the designs of Figs. 1(a)–1(c).

The superior performance of the fishnet design has been already demonstrated in the infrared regime, where the design was first introduced.[10,14] Indeed, the fishnet structure led to the currently lower-loss high-frequency LH materials. As-

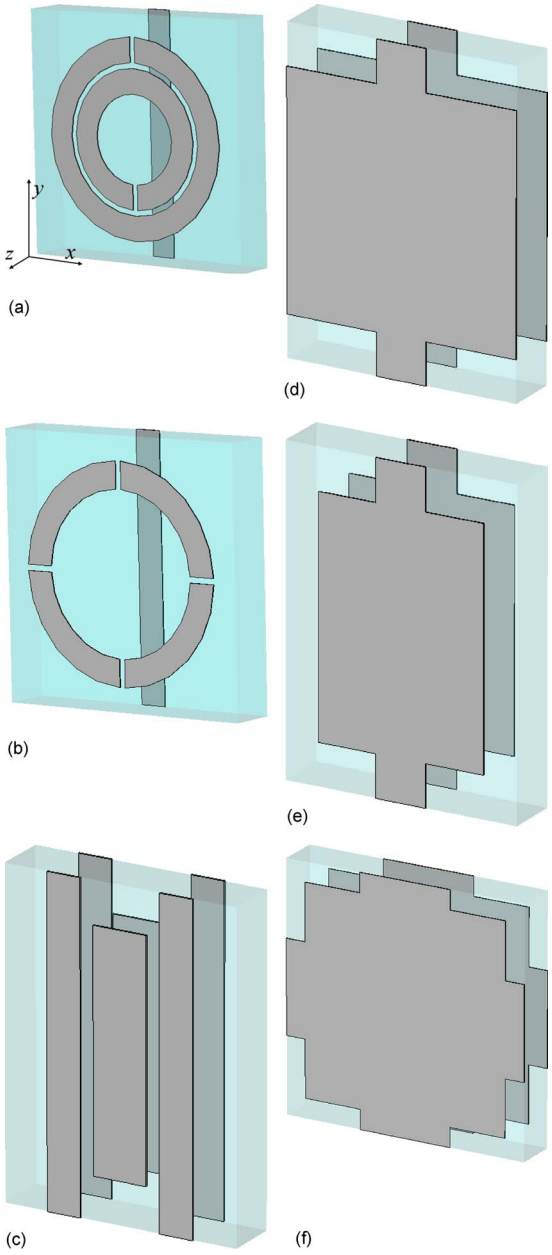

FIG. 1. (Color online) Various unit-cell designs for LH behavior consisting of metals (dark regions) and dielectrics (light semitransparent regions). (a) The design proposed by Pendry *et al.* and implemented by Smith *et al.*: Two single split metallic rings have been deposited on a dielectric on the back side of which a continuous metallic wire is attached. (b) Single ring with one or more cuts (the 4-cut is shown). (c) The cut slab design assisted by continuous wires. (d) The fishnet structure and [(e) and (f)] some of its variations.

sociated parametric study showed negative real part of the refractive index and small imaginary parts over a wide range of structure parameters.

In this paper, we present a systematic study of the fishnet design in the microwave part of the spectrum, attempting to understand the behavior of the design and the origin of its superior performance, mainly its ability to produce LH behavior over a wide range of structure parameters.

The structures shown in Figs. 1(e) and 1(f), which are modifications of the simple fishnet design, have certain advantages over the one in Fig. 1(d). The (e) structure, which will be referred to in the rest of the paper as modified fishnet design, allows the combination of several such double sheets perpendicularly to each other as to create an effective two-dimensional structure, as opposed to a single sheet which works only for one direction of the electromagnetic (EM) field and one polarization. The structure shown in Fig. 1(f) works for one direction of the field but for both polarizations and, hence, for unpolarized waves as well. In the following, it will be referred to as isotropic-like fishnet.

The paper is organized as follows: In Sec. II, we present an experimental and theoretical transmission study of the fishnet design and we demonstrate LH behavior with high transmittance in that design. In Sec. III, we try to analyze the design by studying the distribution of fields and currents at the LH regime. This fields and currents distribution, which show a counterintuitive behavior, lead to the derivation of an effective *LC* circuit description for the design, which we use in Sec. IV to understand the properties of the design and to explain its superior performance. Finally, in Sec. V, we attempt to explain the counterintuitive behavior of fields and currents in the fishnet design.

II. TRANSMISSION RESULTS AND EFFECTIVE MATERIAL PARAMETERS

In Fig. 2, we show simulation and measurement results, in excellent agreement with each other, for the normal incidence electromagnetic wave transmission coefficient through an array of the fishnet structure [Fig. 1(d)].

The structure has been fabricated using a standard printed circuit board process with 30-μm-thick copper patterns on 1.6-mm-thick FR4 dielectric substrates. The measurements have been performed on a system of $18\times13\times3$ unit cells (u.c.) of the structure (3 u.c. along propagation direction), in free space, using an HP 8722 ES network analyzer and microwave standard-gain horn antennas.

The transmission simulations have been performed using the finite integration technique, employed through the MICROWAVE STUDIO commercial software, also considering 3 u.c. of the structure along propagation direction but periodic boundary conditions along the lateral directions.

In both the simulations and measurements, the incident wave is normal to the plane of the fishnet with the electric field parallel to the continuous wire, as shown in the right panel of Fig. 2.

As can be seen in Fig. 2, there is a well-resolved and high intensity transmission peak at around 13 GHz, separated from a high transmission shoulder around 15 GHz by a shallow dip. Inverting the simulated transmission and reflection results to obtain the effective structure parameters,[16] we find that at the ~13 GHz peak (shaded area) both the effective ϵ and μ of the structure are negative, indicating the LH nature of the peak. The effective material parameters for the fishnet structure are shown in Fig. 3, confirming the LH behavior of the structure in the region ~12.3–13.5 GHz.

A more detailed investigation of the structures presented in Fig. 2 showed that the observed −5 dB [for Fig. 2(a)] and

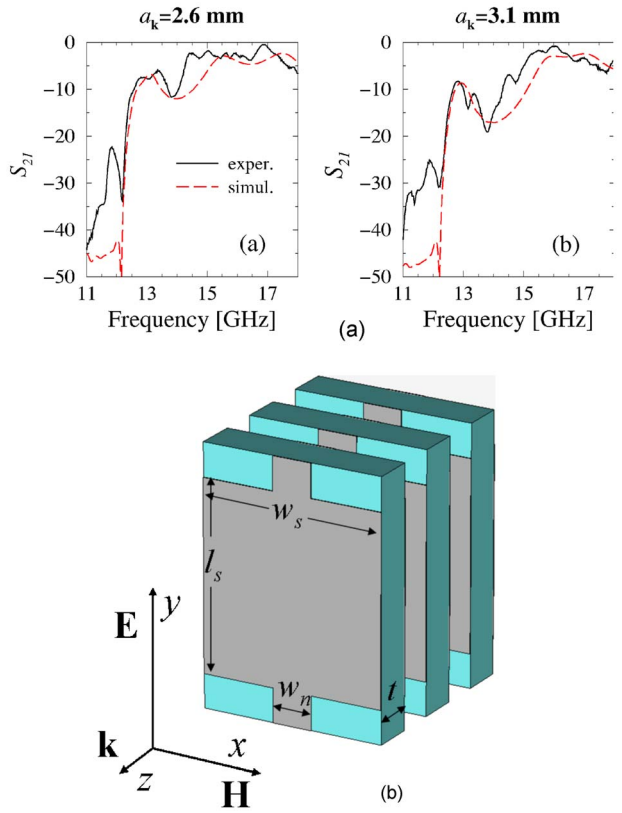

FIG. 2. (Color online) Measured (solid lines) and simulated (dashed lines) electromagnetic (EM) wave transmission (S_{21}) through a set of three unit cells along the propagation direction of the fishnet structure, shown in the right panel of the figure. The unit-cell side along the propagation direction, $a_{\mathbf{k}}$, is 2.6 mm for panel (a) and 3.1 mm for panel (b). The other unit-cell sides are $a_{\mathbf{E}}$=9.5 mm and $a_{\mathbf{H}}$=7 mm. The structure parameters are as follows: continuous wires' width (necks in the fishnet), w_n=1.5 mm; metal thickness, t_m=30 μm; slabs' length, l_s=7 mm; thickness of the dielectric FR4 board separating the metallic elements in each unit cell, t=1.6 mm. The board dielectric constant and conductivity used in the simulations are ϵ_b=4 and σ_b=0.022 S/m. The metal conductivity used is σ_m=5.88×10^7 S/m.

−8 dB [for Fig. 2(b)] reductions of LH transmission are almost exclusively due to losses in the dielectric substrates between the metallic parts. This indicates that a lower-loss substrate could lead to almost 100% LH transmission. [Note that in the slab-pair-based structures, at the magnetic resonance of the structure, the electric-field concentration (large on resonance) is almost exclusively inside the dielectric substrate separating the pair; thus, even a small loss factor of the substrate can lead to large transmission reduction.]

The possibility to obtain almost 100% transmission in our structures by employing a low-loss substrate is demonstrated by the transmission results presented in Fig. 4. Here, we compare the simulated transmission of the fishnet structure used above with those of the structures shown in Figs. 1(e) and 1(f) for 5 u.c. along propagation direction. The parameters of the fishnet structure here are those described in connection with Fig. 2(b) with only difference that the dielectric substrate here has been considered lossless. The differences in the transmission spectra between the regular fishnet and its

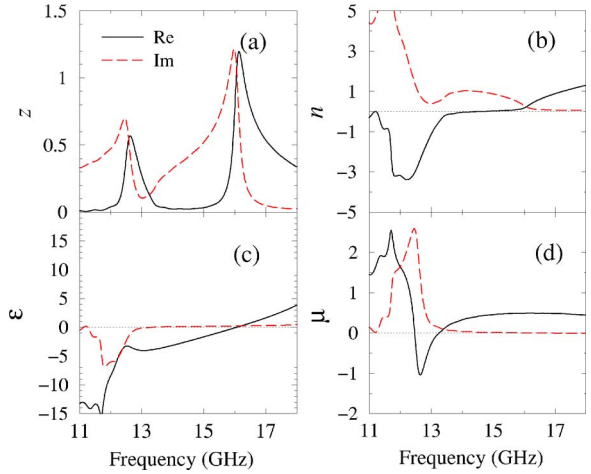

FIG. 3. (Color online) Effective material parameters, impedance (z), refractive index (n), permittivity (ϵ), and permeability (μ) for the fishnet structure of Fig. 2(b). The solid lines show the real part of the parameters, the dashed lines the imaginary part, and the dotted horizontal lines are guides for the eyes.

modification shown in Fig. 1(e) are rather minor: The LH peak in the case of Fig. 1(e) is slightly narrower and at higher frequency in comparison to the connected fishnet structure. These differences will be explained in Sec. III. Detailed study of the structure of Fig. 1(e) showed that it presents the same qualitative behavior as the connected fishnet structure; therefore, the results presented here concerning the fishnet structure are also valid for the modified fishnet. The main advantage of the modified fishnet structure is that it is more appropriate for practical implementation of two-dimensional LH materials, where one needs to combine two perpendicularly aligned arrays of structure layers. The same

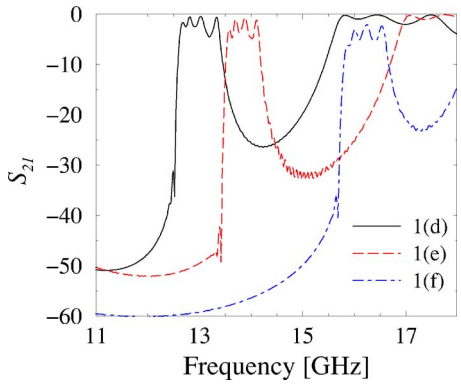

FIG. 4. (Color online) Transmission vs frequency (simulated) for a set of five unit cells along the propagation direction of the fishnet structure shown in Fig. 1(d) (solid line), the modified fishnet design shown in Fig. 1(e) (dashed line), and the isotropic-like fishnet design shown in Fig. 1(f) (dotted dashed line). The parameters for the fishnet and the modified fishnet designs are those mentioned in Fig. 2(b), except that the substrate here has been considered as lossless; the width of the short slabs in the modified fishnet is 5 mm. For the isotropic-like fishnet design, the width of the continuous wires is 3.6 mm, the length of the short slabs l_s is 8 mm, and the unit-cell sides $a_{\mathbf{H}}$=$a_{\mathbf{E}}$ are 9.5 mm. The rest of the parameters are those mentioned in connection with Fig. 2(b).

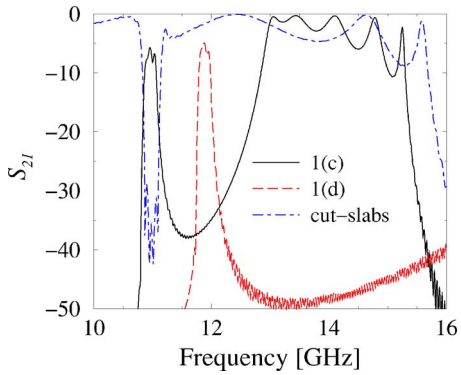

FIG. 5. (Color online) Comparison of the simulated transmission vs frequency of the short slabs (of width of 1.6 mm) combined with continuous wires as shown in Fig. 1(c) (solid line) with the fishnet design of Fig. 1(f) (dashed line). The dotted dashed line shows the transmission for only the short slabs (of width of 1.6 mm); the dip at ~11 GHz is due to the negative permeability response of the slabs. The parameters here are as follows: Substrate thickness (pair separation), t=0.3 mm; unit-cell length along the propagation direction, $a_{\mathbf{k}}$=2.3 mm; width of the continuous wires, w=1 mm; lossless substrate [note that case 1(c) involves two pairs of wires per unit cell, while the fishnet, 1(f), one pair]. The rest of the parameters are those mentioned in connection with Fig. 2.

qualitative behavior as the regular fishnet design is also presented by the isotropic-like fishnet design shown in Fig. 1(f). The advantage of this design, as has been already mentioned, is that it behaves in the same way for arbitrarily polarized wave within the x-y plane.

As was mentioned also in the Introduction, the fishnet structure can be considered as a combination of pairs of short slabs with continuous wires which are physically connected. A thorough investigation of the structure, in comparison with structures based on nonconnected short-slab pairs and continuous wires [like the one shown in Fig. 1(c)],[12] showed that the fishnet combination is an optimized way to obtain LH behavior: it provides negative refractive index over a wide range of structure parameters, and it is associated with good impedance match with the free space, and thus high transmission values, even when the magnetic-resonance frequency lies far below the effective plasma frequency of the system, ω_p'. (We have to point here that to achieve high transmittance in usual LH metamaterials, the magnetic-resonance frequency should lie not far below the effective plasma frequency ω_p'; it should be restricted in a narrow regime just below ω_p'; only this way can it maintain a good impedance, $z=\sqrt{\mu/\epsilon}$, match with the free space.)

For a first demonstration of the superior performance of the fishnet design (which we analyze in the rest of the paper), we compare in Fig. 5 the transmission results of a fishnet structure with that of the structure shown in Fig. 1(c), involving nonconnected pairs of short slabs and continuous wires. Besides the upward shift of the LH peak in the fishnet structure, which will be explained in the next section, a main difference is the clear separation of the LH peak from the nearby broad right-handed peak, maintaining simultaneously high transmission values. Notice that the larger separation between left- and right-handed peaks in the fishnet, indicating a higher plasma frequency ω_p', cannot be explained only by the continuous wire contribution to the effective ϵ, since in the nonconnected case there are two pairs of wires per unit cell, expected to give a much larger ω_p' than in fishnet where only one pair is employed. This paradox can be explained only by taking into account the influence of the electric response of the pair[11] on ω_p', as was discussed in the Introduction. As we will show in Sec. IV, this influence, which leads to a downward shift of ω_p' and steeper $\epsilon(\omega)$ dispersion, is smaller if the slabs are of larger width and it remains small if the slabs are connected with continuous wires.

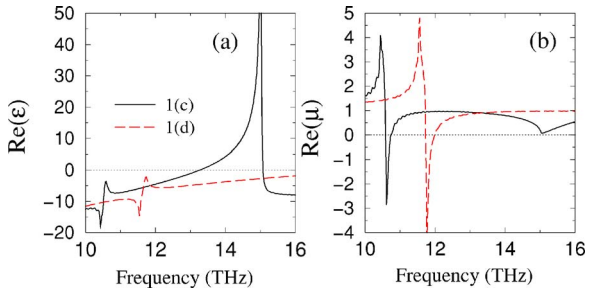

FIG. 6. (Color online) Effective material parameters ϵ and μ, for the slab and wire structures of Fig. 5. Solid lines are for the structure of the nonconnected slabs and wires [shown in Fig. 1(c)], while dashed lines are for the fishnet structure [shown in Fig. 1(d)]. The dotted horizontal lines are guides for the eyes. Note that the antiresonances in the parameters are artifacts coming from the periodicity of the structure, which imposes an upper limit to the retrieved refractive index from which ϵ and μ are simulated (Ref. 17).

The effective ϵ and μ parameters calculated from the transmission data of Fig. 5 (and from the associated reflection data), which are shown in Fig. 6, are in support of the above reasoning. Indeed, as one can see from Fig. 6(a), the effective plasma frequency is lower in the nonconnected case, while a resonant structure appears (at ~15 GHz), due to the cut-wire-like electric response of the slabs,[11] making the ϵ dispersion close to the magnetic resonance more steep. This steep $\epsilon(\omega)$ imposes tight limits in the optimum position for the magnetic-resonance frequency as to achieve good impedance match with the free space and thus high transmission values.

This is not the case though for the fishnet design, where a smooth, Drude-like $\epsilon(\omega)$ response is observed, with slowly varied $\epsilon(\omega)$, allowing a good impedance match possibility over a wide range below the plasma frequency ω_p'. This smooth $\epsilon(\omega)$ response, explained in Sec. IV, is one of the main reasons that make the fishnet design functional for a wide range of structure parameters.

III. FIELDS AND CURRENTS DISTRIBUTION AND EFFECTIVE CIRCUIT DESCRIPTION

A. Fields and currents distribution

Attempting to analyze the fishnet structure and to understand further its observed superior performance compared to other designs involving nonconnected short-slab pairs and continuous wires, we examined the field and current distri-

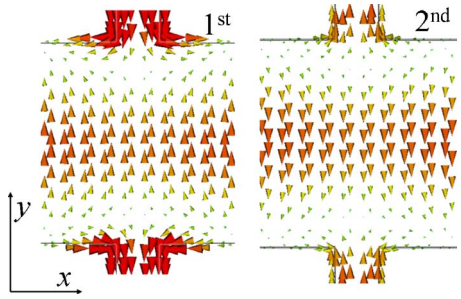

FIG. 7. (Color online) Surface current distribution for the fishnet structure presented in Fig. 2(b) (single pair along the propagation direction) at frequency just above the magnetic resonance. The incoming EM field meets first the surface indicated as 1st in the plot.

bution at the magnetic-resonance frequency and at the other characteristic frequencies of the structure.

In Fig. 7, we show the surface current distribution for the structure presented in Fig. 2(b) at the inner (facing each other) metallic surfaces of the structure, at a frequency just above the magnetic resonance ($f=\omega/2\pi=12.5$ GHz). We consider here one unit cell of the structure in propagation direction (z direction) and periodic conditions along the lateral ones. The metallic conductivity has been taken as 5.88×10^7 S/m, which leads to skin depth value (1 μm) much smaller than the metal thickness, hence practically zero. The most surprising feature in Fig. 7 is that the currents at the neck regions are opposite to those of the slab areas, producing thus a strong charge accumulation at the areas where the two opposing flowing currents meet each other. A possible explanation for this counterintuitive behavior will be postponed for Sec. V. The other characteristic feature, i.e., opposite currents at the two wires constituting the pair, is the one responsible for the resonant magnetic response of the pair and it is essentially the same with what one observes in the case of isolated short-wire pairs.

To validate the observed current distribution and to examine further where the charge accumulation actually occurs, we examined the fields at the same frequency at which the

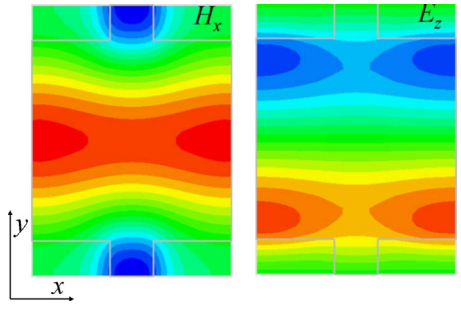

FIG. 8. (Color online) The magnetic-field component H_x for the fishnet structure of Fig. 2(b) (left panel) and the electric-field component E_z (right panel) just above the magnetic-resonance frequency of the structure. Propagation is along the z direction. Red color indicates strong positive values and blue strong negative values. The displayed fields are calculated at an x-y plane located in the middle between the two sheets of the pair along the z direction and at a frequency just above the magnetic-resonance frequency of the structure.

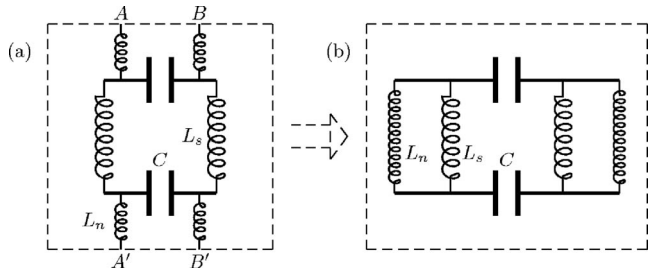

FIG. 9. An LC circuit model for the fishnet structure. L_s and L_n denote the loop inductances at the slabs and necks, respectively, and C the capacitance of the structure. The right panel results from left panel after taking into account the periodicity and thus the equivalence of the points A and A' and B and B'.

currents were calculated. In Fig. 8, we show the dominant field components, H_x (**H** component in the direction of the external magnetic field) and E_z (**E** component along propagation direction; E_z is proportional to surface charge density). One can see that the magnetic-field distribution is consistent with the current distribution observed in Fig. 7, demonstrating the antiparallel currents between slabs and necks. The currents in the necks are also antiparallel to one another between the two sheets of the fishnet pair, amounting thus to a magnetic response also at the neck parts, as can be seen from the strong H_x values between the necks. The magnetic response of the necks in the fishnet structure is opposite to the magnetic response of the slabs and can be taken into account in an effective LC description of the structure by introducing an additional inductance, as we will show later on in this section.

Examining the E_z distribution shown in the right panel of Fig. 8, which is also consistent with the current distribution of Fig. 7, one can additionally observe that the accumulation of charges in the fishnet design is not uniform along the upper and lower edges of the slabs, as in isolated slab pairs, but it takes place mainly at the x edges of the unit cell (see Fig. 8).

B. Effective *LC* circuit description of the fishnet structure

From the currents and fields distribution observed in Figs. 7 and 8, one can draw a simple effective LC circuit model describing the fishnet structure close to the magnetic-resonance regime, useful for further analysis and understanding of the structure. This model will look like the LC model describing a system of short-slab pairs,[15] with an additional inductance representing the magnetic response of the necks. A drawing of such a model for one unit cell of the fishnet structure is shown in Fig. 9. Figure 9(a) gives a schematic of the model that directly corresponds to the geometry of the structure; there, L_s and L_n represent the inductance arising from the looplike currents at the slabs and the necks, respectively, and C the capacitance between the two slabs. Taking into account the periodicity, and thus the equivalence of the points A (B) and A' (B'), the model of Fig. 9(a) can be transformed to the simpler and more appropriate for calculations model that is shown in Fig. 9(b). Notice that the antiparallel currents between slabs and necks which have been

observed for the fishnet structure correspond to parallel currents in the parallel connected inductances L_s and L_n of Fig. 9(b).

Taking into account the effective *LC* circuit description of the fishnet structure, as is shown in Fig. 9(b), the magnetic-resonance frequency of the structure, ω_m, can be written as

$$\omega_m^2 = \frac{1}{LC} = \frac{1}{L_s C} + \frac{1}{L_n C} \approx \omega_{m(\text{short-slabs})}^2 + \frac{1}{L_n C}, \tag{1}$$

where $\omega_{m(\text{short-slabs})}$ is the magnetic-resonance frequency for only the pairs of short slabs and the approximation in the last equality is due to the fact that the capacitance in the fishnet is expected to be slightly modified compared to that of the only short-pair structure, due to the nonuniform charge distribution in the fishnet. From Eq. (1), it is easy to see that the magnetic-resonance frequency of the fishnet is shifted upward compared to the magnetic-resonance frequency of only the short-slab pair involved in the structure; this upward shift is mainly due to the inductance of the necks. The higher magnetic-resonance frequency of the fishnet is verified by the transmission results presented in Fig. 5, comparing the fishnet structure with one of nonconnected slab pairs and wires. This higher frequency is nicely explained by Eq. (1).

IV. CHANGING THE GEOMETRY AND THE TOPOLOGY

In this section, we attempt a parametric study of the fishnet structure, essential for any attempts for structure optimization and for the understanding of the results and some of the paradoxes that have been presented in the previous sections. For a qualitative analysis and explanation of the results of this study, we will use the *LC* description of the structure, given in Eq. (1), with the slabs capacitance given by the simple formula

$$C \sim \frac{S}{t} \tag{2}$$

(capacitance of a parallel-plate capacitor of plate area S, proportional to the actual area $w_s l_s$, and plate separation t), and the loop inductances by the solenoid's inductance formula, i.e.,

$$L_s \sim \frac{l_s t}{w_s}, \quad L_n \sim \frac{l_n t}{w_n}, \tag{3}$$

for the slab and neck inductances, respectively; in the above formulas, w_n (w_s) is the width of the neck (slab), as is shown in the right panel of Fig. 2, l_n (l_s) is the corresponding length, and t is the separation distance between the two sheets of the fishnet pair. [Note that Eqs. (3) can also be used for semiquantitative simulations, if one replaces the lengths appearing by equivalent effective lengths, proportional to the actual lengths though.]

Since the neck and the slab inductances are in parallel, the inverse of the total inductance L of the fishnet is of the form

$$\frac{1}{L} \sim \frac{w_n}{l_n t} + \frac{w_s}{l_s t}, \tag{4}$$

leading to a magnetic-resonance frequency of the form

$$f_m = \frac{\omega_m}{2\pi} \sim \sqrt{\frac{1}{l_s^2} + \frac{1}{l_s l_n}\frac{w_n}{w_s}}. \tag{5}$$

As we will show in the next sections, Eq. (5) is able to account for the influence of all the geometrical parameters on the magnetic-resonance frequency of the fishnet.

A. Reducing the slab's width

Equation (5) suggests that by reducing the width of the slabs, w_s, the frequency f_m must increase. Indeed, transmission simulations verify this increase and are in semiquantitative agreement with the simple formula (5). A verifying example is shown in the transmission results of Fig. 4 (compare the solid and dashed lines, where the only different parameter is the slab width).

Another observation that can be deduced from Eq. (5) is that what causes the upward shift of the magnetic-resonance frequency of the fishnet as one decreases the slab's width is actually the presence of the necks. For slab pairs only, i.e., $w_n = 0$ in Eq. (5), the slab's width does not influence the magnetic-resonance frequency of the slabs, as is discussed in Ref. 15 and was also verified by related transmission simulations.

Finally, we have to mention that approaching the limit $w_s \to w_n$, where the system tends to reduce to pairs of infinite parallel wires which are not expected to sustain any resonance, the magnetic resonance becomes more and more weak (due to the reduction of the available area for the induced magnetic field[2]) and tends to disappear as $w_s \to w_n$, as is revealed by detailed transmission simulations.

B. Reducing the neck's width

Reducing the neck's width in the fishnet, one increases the neck inductance [see Eqs. (1) and (3)]; thus, the magnetic-resonance frequency of the system is expected to go to lower values, approaching the resonance frequency of the only slab-pair case. This can be seen in Eq. (5) when $w_n \to 0$ and is verified by transmission simulations.

On the other hand, since the necks in the fishnet serve as continuous wires and essentially determine the plasma frequency of the system, by reducing the neck's width (i.e., reducing the width of the continuous wires) one decreases the plasma frequency of the system, ω_p'. Thus, for a given unit-cell size of a LH fishnet system and given slabs' length, l_s, the neck width determines essentially the distance between the LH peak and the neighboring right-handed transmission regime, a factor critical for the effective impedance ($z = \sqrt{\mu/\epsilon}$) of the structure.

C. Electric response of the fishnet structure

In this section, we discuss the electric response of the fishnet structure and we show that it is essentially the electric

response of the continuous wires (necks) included in the structure.

As has been mentioned earlier, the electric response of a system like the ones shown in Figs. 1(a)–1(c) is not only determined by the Drude-like response of its continuous wires; one has to take into account also the resonant dipole-like (or short-wire-like) electric response of the structures producing the magnetic response, i.e., the SRRs or the short wires. The consideration of this response (with resonance not far from the magnetic-resonance frequency) results to a reduction of the effective plasma frequency of the system and to a steeper $\epsilon(\omega)$ dispersion; thus, it makes more difficult the achievement of LH behavior and the impedance match condition. (The effective ϵ of a LH system can be obtained by adding the short-wire Lorenz-type effective ϵ of the magnetic structures to the Drude-like effective ϵ of the continuous wires.[11] The actual plasma frequency of the combined system is lower than both ω_p of wires only and the short-wire-like electric resonance frequency ω_e of the "magnetic structures.") This reduction of the plasma frequency compared to that of only wires is stronger the lower the frequency ω_e is. Therefore, it is favorable to keep the short-wire-like electric response of the system at as high frequencies as possible. As we show below, in a slab pair and wire system this can be achieved either by employing wide slabs (large w_s) or by connecting slabs and wires. Fishnet design exploits both possibilities.

For a system of short-slab pairs, the frequency ω_e depends not only on the length of the slabs but also on their width. This can become evident if one describes such a system close to the electric resonance with an effective LC circuit, following the spirit of Ref. 15, with $\omega_e = 1/\sqrt{L_e C_e}$, where L_e is the straight wire inductance of a slab of the pair and C_e the capacitance between neighboring slabs along the external **E** direction.

$$C_e \propto w_s, \quad L_e \propto \ln(l_s/w_s). \tag{6}$$

By increasing the slab's width w_s (being lower than the length l_s), the decrease of the inductance L_e dominates over the increase of the capacitance C_e and this results to an increase of the frequency ω_e, as is verified by transmission simulations and effective parameters determination. (Note that for isolated slabs the magnetic-resonance frequency, ω_m, does not depend on w_s; thus, wider slabs correspond to larger ω_m-ω_e separation.) For practically achievable unit-cell sizes in the GHz range, the frequency ω_e of short slabs with width close to the one of the unit cell lies well above the magnetic-resonance frequency ω_m and usually above the plasma frequency of any continuous wires needed to produce LH behavior; therefore, it does not affect much the low-frequency electric response of the continuous wires. On the other hand, for narrow slabs like the ones involved in system 1(c) of Fig. 5, ω_e lies below the wires' plasma frequency, ω_p, and essentially determines the total plasma frequency, ω_p', of the system. [For the specific system 1(c) of Fig. 5, $f_e = \omega_e/2\pi \approx 16$ GHz, $f_p = \omega_p/2\pi \approx 33$ GHz, and $f_p' = \omega_p'/2\pi \approx 13$ GHz.] This explains the lower ω_p' and steeper $\epsilon(\omega)$ dispersion of system 1(c) observed in Figs. 5 and 6 compared to the fishnet design, system 1(d).

For the fishnet-like designs (i.e., connected slabs and wires), there is an additional related advantage, stemming from the physical connection of slabs and wires: Examining the currents in the fishnet structure immediately after the frequency ω_e, we again observe antiparallel currents between slabs and necks, suggesting that the effective linear inductance of the necks is again in parallel with the inductances L_e of the slabs. Therefore, ω_e^2 here is proportional to $A/[w_s \ln(l_s/w_s)] + B/[w_s \ln(l_n/w_n)]$ (A and B are constants, depending on the other parameters of the system). In the last relation, the decrease of the second term in the sum (as a result of increasing w_s) counteracts the increase of the first one and this leaves the electric resonance frequency almost unaffected.

Therefore, the effective electric response of the fishnet design is actually the Drude-like electric response of the continuous wires only. As was mentioned in Sec. II, this effect is associated with an advantage for the LH behavior of the structure, stemming from the fact that the Drude-like effective ϵ experiences slower changes than an effective ϵ influenced by electric resonances. This, combined with the fact that the effective permeability does not take large negative values, has as result a more wide frequency regime where good impedance match with the free space can be achieved, and thus high LH transmittance values.

D. Changing the length of the neck

As shown in Fig. 10, by increasing the length of the neck, the main effect is the following: The region where the opposite running currents come to a head-on collision moves from inside the slabs (see Figs. 7 and 8) to the neck area (Fig. 10).

This effective lengthening of the current flow both in the slab and in the rest of the neck increases the inductance (which is proportional to the effective length) and, to a smaller degree, the capacitance; as a result the magnetic-resonance frequency is expected to be reduced as the length of the neck increases, in agreement with the simulation results. (The magnetic-resonance frequency of the structure of Fig. 10 is at ~9 GHz, while that for the structure of Fig. 8 is at ~12.5 GHz.)

V. DISCUSSION

We now return to the question of how one can understand the opposite flowing currents in the neck and the slab of the fishnet design. One way to think about this problem is to realize first that the line AB and the line $A'B'$ in Fig. 11(a) are identical. This is so because the periodicity implies Bloch's theorem, stating that the solution $F(\mathbf{r})$ has the form

$$F(\mathbf{r}) = u(\mathbf{r})e^{i\mathbf{kr}}, \tag{7}$$

where $F(\mathbf{r})$ is any component of the EM field and the current, $u(\mathbf{r})$ is a periodic function of $\mathbf{r}$ in the x-y plane (see Fig. 2 for the coordinate system), and $\mathbf{kr} = kz$ since $\mathbf{k}$ is along the z direction. Hence, $F(\mathbf{r})$ is a periodic function of x and y, and A and A' are equivalent. As a result, we can redraw the metallic sheets of the fishnet design as in Fig. 11(b) or 11(c), creating thus a closed loop consisting of two distinct ele-

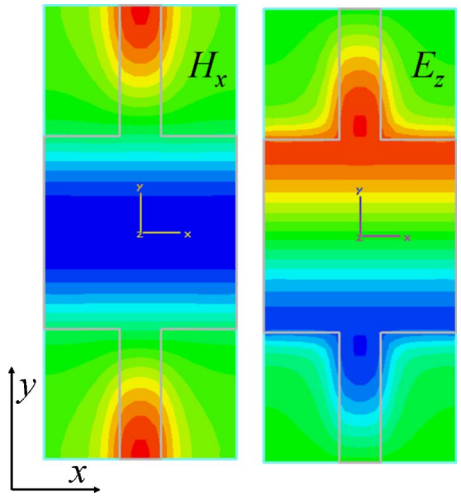

FIG. 10. (Color online) The magnetic-field component H_x (left panel) and the electric-field component E_z (right panel) just above the magnetic-resonance frequency ($\omega_m \approx 9$ GHz) for a fishnet structure with those parameters mentioned in Fig. 2, except the unit-cell side $a_{\mathbf{E}}$, which here is 16.5 mm, thus increasing the length of the neck part of the structure. The displayed fields are calculated at an x-y plane located in the middle between the two sheets of the pair, and at a frequency just above the magnetic-resonance frequency of the structure. Propagation is along the z direction. Red color indicates large positive values and blue color large negative values.

ments: the slab and the neck. There are at least two distinct ways for current to flow in this two-component loop: either in opposite directions (topologically), as in Fig. 11(b), or at the same direction, as in Fig. 11(c). Both modes are admissible; the current distribution in the fishnet is in general a superposition of (at least) these two current modes. The basic difference between the two modes is that the first one creates charge accumulation where the opposite currents in slab and neck meet, while the second is just a circular current without charge accumulation. The first mode is easily identified with the resonant oscillatory modes of the slab: the magnetic resonance which has opposite polarization of the corresponding slabs in the two sheets of a single fishnet unit cell, and the electric short-wire response where the corresponding slabs are polarized in the same direction. Charge conservation enforces pairwise spatial charge accumulations with opposite sign, the capacitance of which constituted the back-driving force in the resonant oscillation. (For the magnetic resonance, this capacitance is predominantly between the sheets, while for the electric resonance, at higher frequency, between the ends of the slabs within a sheet.) There may occur higher-order resonant modes with four or more current nodes (charge accumulation) but those have much higher resonance frequencies and are not of interest here.

The second mode, as nonresonant (no charge accumulation, no capacitance) current, can be identified with the plasmonic electric response of the "continuous wires" constituted by the connection of slabs and necks. Those wires are simply polarized by the external electric field, which gives rise to a linear electric (polarization) current through slabs and necks in the same direction (and, moreover, in parallel in both

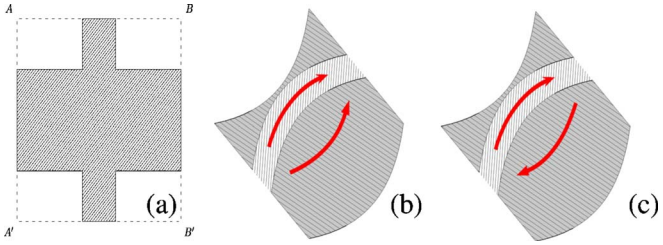

FIG. 11. (Color online) (a) Schematics of one unit cell of the fishnet design. Dashed lines show the boundaries of the unit cell. Due to the periodicity, the lines AB and $A'B'$ are equivalent. Panels (b) and (c) are redrawings of the metallic sheet of panel (a) taking advantage of the periodicity, and drawing also the two possibilities for current flow: (b) topologically opposite direction current flow and (c) topologically same direction flow.

sheets of the fishnet layer). In the vicinity of the magnetic response of the fishnet structure, these plasmonic currents are usually much weaker than those of the resonant mode. Therefore, the field and current distribution snapshots (Figs. 7 and 8) apparently only reveal the antiparallel behavior of the currents in slabs and necks. The reader may have noticed the slightly different magnitude of the antiparallel currents in the two sheets in Fig. 7. This asymmetry originates from the superimposed nonresonant currents which flow parallel in both sheets and add to or subtract from the antiparallel currents.

We should mention that for the two resonant modes, both capacitance (in between sheets vs simultaneously along the slabs within the sheets) and effective inductance are different for magnetic and electric resonances. The larger intersheet capacitance together with the (usually) larger loop inductance for the antiparallel currents in the sheets explains the lower eigenfrequency, f_m, of the magnetic resonance compared to f_e for the electric resonance.

VI. CONCLUSIONS

We have performed a systematic study of the fishnet structure and its modified versions, all of which produce strong, well-resolved LH behavior. The version shown in Fig. 1(f) is expected to work equally well for unpolarized and polarized EM waves. The counterintuitive current and field distributions leading to the desired performance were analyzed and clarified. The role of the various geometrical parameters on the LH behavior of the structure was examined and the results of the simulations were accounted for by employing the effective capacitor-inductor circuit description of the structure.

ACKNOWLEDGMENTS

The authors acknowledge the financial support by the EU grants LSHG-CT-2003-503259, METAMORPHOSE, and PHOREMOST, by Ames Laboratory (Contract No. DE-AC02-07CH11385), DARPA (Contract No. MDA-972-01-2-0016), AFOSR (MURI Grant No. FA955-06-1-0337), and by the Greek Ministry of Education (Pythagoras Project).

[1] V. G. Veselago, Sov. Phys. Usp. **10**, 509 (1968) [Usp. Fiz. Nauk **92**, 517 (1967)].
[2] C. M. Soukoulis, M. Kafesaki, and E. N. Economou, Adv. Mater. (Weinheim, Ger.) **18**, 1941 (2006).
[3] D. R. Smith, W. J. Padilla, D. C. Vier, S. C. Nemat-Nasser, and S. Schultz, Phys. Rev. Lett. **84**, 4184 (2000).
[4] J. B. Pendry, A. J. Holden, D. J. Robbins, and W. J. Stewart, IEEE Trans. Microwave Theory Tech. **47**, 2057 (1999).
[5] J. B. Pendry, A. J. Holden, W. J. Stewart, and I. Youngs, Phys. Rev. Lett. **76**, 4773 (1996); J. B. Pendry, A. J. Holden, D. J. Robbins, W. J. Stewart, J. Phys.: Condens. Matter **10**, 4785 (1998).
[6] R. A. Shelby, D. R. Smith, and S. Schultz, Science **292**, 77 (2001).
[7] K. Aydin, K. Guven, M. Kafesaki, L. Zhang, C. M. Soukoulis, and E. Ozbay, Opt. Lett. **29**, 2623 (2004).
[8] V. M. Shalaev, W. S. Cai, U. K. Chettiar, H. K. Yuan, A. K. Sarychev, V. P. Drachev, and A. V. Kildishev, Opt. Lett. **30**, 3356 (2005).
[9] G. Dolling, M. Wegener, C. M. Soukoulis, and S. Linden, Opt. Lett. **32**, 53 (2007); G. Dolling, C. Enkrich, M. Wegener, C. M. Soukoulis, and S. Linden, *ibid.* **31**, 1800 (2006).
[10] S. Zhang, W. Fan, N. C. Panoiu, K. J. Malloy, R. M. Osgood, and S. R. J. Brueck, Phys. Rev. Lett. **95**, 137404 (2005).
[11] T. Koschny, M. Kafesaki, E. N. Economou, and C. M. Soukoulis, Phys. Rev. Lett. **93**, 107402 (2004).
[12] J. Zhou, L. Zhang, G. Tuttle, Th. Koschny, and C. M. Soukoulis, Phys. Rev. B **73**, 041101(R) (2006).
[13] K. Guven, M. D. Caliskan, and E. Ozbay, Opt. Express **14**, 8685 (2006).
[14] S. Zhang, W. Fan, K. J. Malloy, S. R. Brueck, N. C. Panoiu, and R. M. Osgood, Opt. Express **13**, 4922 (2005).
[15] J. Zhou, E. N. Economou, Th. Koschny, and C. M. Soukoulis, Opt. Lett. **31**, 3620 (2006).
[16] D. R. Smith, S. Schultz, P. Markoš, and C. M. Soukoulis, Phys. Rev. B **65**, 195104 (2002); T. Koschny, P. Markoš, D. R. Smith, and C. M. Soukoulis, Phys. Rev. E **68**, 065602(R) (2003).
[17] Th. Koschny, P. Markos, E. N. Economou, D. R. Smith, D. C. Vier, and C. M. Soukoulis, Phys. Rev. B **71**, 245105 (2005).